Thermal Decomposition of NCN: Shock-Tube Study, Quantum Chemical Calculations, and Master-Equation Modeling

Anna Busch,[†] *Núria González-García,*[†] *György Lendvay,*[‡] *and Matthias Olzmann**[†]

[†]Institut für Physikalische Chemie, Karlsruher Institut für Technologie (KIT), Kaiserstr. 12, 76131 Karlsruhe, Germany

[‡]Institute of Materials and Environmental Chemistry, Research Center for Natural Sciences, Hungarian Academy of Sciences, Magyar Tudósok krt. 2., Budapest H-1117, Hungary

To be published in The Journal of Physical Chemistry A

Abstract

The thermal decomposition of cyanonitrene, NCN, was studied behind reflected shock waves in the temperature range 1790–2960 K at pressures near 1 and near 4 bar. Highly diluted mixtures of NCN_3 in argon were shock-heated to produce NCN, and concentration-time profiles of C atoms as reaction product were monitored with atomic resonance absorption spectroscopy at 156.1 nm. Calibration was performed with methane pyrolysis experiments. Rate coefficients for the reaction $^3NCN + M \rightarrow {}^3C + N_2 + M$ (R1) were determined from the initial slopes of the C-atom concentration-time profiles. Reaction R1 was found to be in the low-pressure regime at the conditions of the experiments. The temperature dependence of the bimolecular rate coefficient can be expressed with the following Arrhenius equation: $k_1^{bim} = (4.2 \pm 2.1) \times 10^{14}$ exp[–242.3 kJ mol^{-1}/(RT)] cm^3 mol^{-1} s^{-1}. The rate coefficients were analyzed by using a master equation with specific rate coefficients from RRKM theory. The necessary molecular data and energies were calculated with quantum chemical methods up to the CCSD(T)/CBS//CCSD/cc-pVTZ level of theory. From the topography of the potential energy surface, it follows that reaction R1 proceeds via isomerization of NCN to CNN and subsequent C−N bond fission along a collinear reaction coordinate without a tight transition state. The calculations reproduce the magnitude and temperature dependence of the rate coefficient and confirm that reaction R1 is in the low-pressure regime under our experimental conditions.

Keywords: Cyanonitrene radical; Combustion; Atom resonance absorption spectroscopy; Unimolecular reactions; Statistical rate theory.

1. Introduction

The cyanonitrene radical, NCN, is considered to be an important intermediate in the formation of so called prompt NO in fuel-rich zones of hydrocarbon flames.[1–9] There is by now a strong evidence that NCN is formed under these conditions in the reaction $CH + N_2 \rightarrow NCN + H$.[1,10,11] Kinetic data of NCN reactions, however, which are of crucial importance for an assessment of the role of NCN in prompt-NO formation, are scarce.[12]

A number of bimolecular NCN-consuming reactions have been proposed and studied over the last few years.[13–17] In addition, the unimolecular decomposition of NCN may also be a relevant loss-channel at sufficiently high temperatures. Theoretical analyses have shown[18] that the latter reaction mainly leads to $C + N_2$ that is, the major thermal decomposition channel of ground state triplet NCN can be written, in bimolecular form, as:

$$^3NCN + M \rightarrow {}^3C + {}^1N_2 + M \qquad \text{(R1)}$$

In early theoretical studies[18,19], besides the linear NCN also a cyclic intermediate, *c*-NCN, and a linear constitutional isomer, CNN, have been identified as minima on the CN_2 triplet potential energy surface (PES). These minima and the transition states connecting them were characterized by a number of quantum chemical methods.[18,19] On the basis of these results, in ref 18 rate coefficients of the different unimolecular reaction pathways of NCN were obtained from multichannel variational RRKM theory. For reaction R1 the following temperature dependence of the first-order rate coefficient was predicted in the temperature range 700–4500 K at a pressure of 1.33 mbar with argon as bath gas:[18] $k_1(P = 1.33\ \text{mbar}) = 3.96 \times 10^{24}\ (T/\text{K})^{-4.74}\ \exp(-41714\ \text{K}/T)\ \text{s}^{-1}$, which results in a bimolecular rate coefficient of $k_1^{\text{bim}} = 2.47 \times 10^{29}\ (T/\text{K})^{-3.74}\ \exp(-41714\ \text{K}/T)\ \text{cm}^3\ \text{mol}^{-1}\ \text{s}^{-1}$. Analogous expressions for pressures of 133 mbar and

1013 mbar are also given in ref 18. From these calculations it follows that k_1 in the above given temperature range is very close to its low-pressure limit even at pressures near 1 bar.[18]

Very recent theoretical studies on the kinetics of the N + CN reaction[20,21] and on roaming pathways in the NCN-CNN isomerization[22] have essentially confirmed the topography of the CN_2 potential energy surface found in the earlier studies.

The kinetics of the thermal unimolecular decomposition of NCN was experimentally studied very recently by Dammeier et al.[15]. Analogous to parallel work from our laboratory,[23,24] these authors used shock heating of NCN_3 to produce NCN radicals.[25,26] They monitored absolute concentration-time profiles of NCN with narrow-bandwith laser absorption at 329.1202 nm. From modeling with a small NCN pyrolysis mechanism (9 reversible reactions, 7 species), the following temperature dependence of the rate coefficient of reaction R1 was inferred for temperatures between 2012 and 3248 K at pressures ranging from 703 to 2204 mbar with argon as bath gas:[15] $k_1^{\text{bim}} = 8.9 \times 10^{14} \exp[-260 \text{ kJ mol}^{-1}/(RT)] \text{ cm}^3 \text{ mol}^{-1} \text{ s}^{-1}$ (uncertainty ±20%). No pressure dependence of the bimolecular rate coefficient was observed, which indicates that k_1 is close to the low-pressure limit under these conditions in line with the predictions mentioned above.

In the present work, we report on a complementary shock-tube study of NCN decomposition. Whereas in ref 15 time-resolved laser absorption was used to monitor the reactant NCN, we use atomic resonance absorption spectroscopy (ARAS)[27,28] to monitor C atoms formed as products of reaction R1. Besides the direct detection of a product, which could verify the predicted dominance of the C + N_2 channel, the high sensitivity of ARAS enables us to apply very low initial concentrations of NCN, which suppresses competing bimolecular reactions.

We analyze our results, using statistical rate theory and model the observed temperature and pressure dependence of the rate coefficient with a master equation on the basis of specific rate coefficients from RRKM theory.[29,30] For the energies and molecular properties needed, we performed quantum chemical calculations which also enables us to validate earlier mechanistic suggestions. In particular, we found that the saddle point for carbon-atom loss from CNN detected at a bent CNN configuration by Moskaleva and Lin[18] does exist, but that there is also a barrierless decomposition pathway lower in energy along a collinear CNN pathway.

2. Experimental Section

The experiments were performed in a honed stainless steel shock tube behind reflected shock waves at temperatures between 1790 and 2960 K and pressures near 1 bar and near 4 bar with Ar as bath gas. NCN was produced from thermal decomposition of NCN_3,[23−26] and the initial concentrations, $[NCN_3]_0$, were in the ranges 2–8 ppm (52 experiments) and 15–33 ppm (19 experiments). The carbon-atom concentration-time profiles were monitored by ARAS at a wavelength of 156.1 nm,[31,32] and the rate coefficients were determined from the initial slopes. The detailed reaction conditions along with the rate coefficients are listed in Tables S1 and S2 of the Supporting Information. In the following a brief description of the experimental setup is given.

2.1. Shock Tube. The shock tube used is identical to that described in earlier publications (see e.g. ref 33 and literature cited therein). A thin aluminium foil divides it in a 3.05 m long high-pressure section and a 4.20 m long low-pressure section. The inner diameter is 10 cm. For the optical detection, there are two MgF_2 windows (diameter: 12 mm, thickness: 2 mm) in the low-

pressure section 5.3 cm away from the end plate. Before each experiment, the whole shock tube was evacuated to pressures of approximately 10^{-6} mbar, and the low-pressure section was filled with the test gas *i.e.*, NCN_3 or CH_4 (the latter for the calibration, see below), highly diluted in argon (99.9999 %, Air Liquide). Hydrogen (99.9 %, Air Liquide) was used as driver gas to initiate the shock wave by pressure bursting of the aluminium foil. By varying the initial pressure in the low-pressure section and the thickness of the aluminium foil, different post-shock temperatures and pressures could be obtained. We used a 30 μm or a 100 μm thick aluminium foil for the experiments at around 1 bar and 4 bar, respectively. The familiar one-dimensional conservation equations were used to calculate the post-shock conditions.[34] To this end, the pre-shock temperature and pressure as well as the velocity of the shock wave have to be known. The initial pressure of the test gas was determined with a Baratron manometer (MKS, 622AX13MDE), and the velocity of the incident shock wave was measured with four fast piezo-electric pressure transducers (Kistler, 603B). Since the mixtures contained only a few ppm NCN_3 or CH_4, the test gas could be treated in the calculations as being pure argon. Consideration of the vibrational heat capacities of the polyatomic compounds had no effect on the calculated post-shock conditions (for vibrational frequencies of NCN_3 see ref 35).

The test-gas mixtures were prepared manometrically in two different 100 L mixing vessels made of stainless steel. Before the preparation of each mixture, the vessels were evacuated to pressures of approximately 10^{-7} mbar. The pressure of NCN_3, CH_4, and the total pressure after the dilution with Ar were measured with two different Baratron manometers (MKS, 626AX02MDE and 626AX13MDE). The mixtures were allowed to homogenize for at least 15 hours before use.

2.2. Atomic Resonance Absorption Spectroscopy. For the ARAS detection, a microwave-powered discharge lamp was attached to the shock tube. The emitted UV light passed the shock tube through the MgF_2 windows, was filtered with a vacuum UV monochromator (Acton Research Corporation, Spectra Pro VM-504), and its intensity was monitored by a solar-blind photomultiplier tube (Hamamatsu, R1259). The signal was recorded in a digital storage oscilloscope (Tektronix, TDS 5104B). The discharge lamp consisted of a quartz tube that was flushed with a suitable gas mixture (1% CO in He) and equipped with an Evenson cavity connected to a microwave generator (Muegge, MW-GPR YJ 1511-300-01) operating at 2.45 GHz. The power was adjusted to 150 W, and the pressure in the lamp was kept at about 8 mbar. By narrow vertical slits (1 mm) at the MgF_2 windows, a time resolution of less than 5 μs could be achieved.

The C atoms were detected at a wavelength of λ = 156.1 nm corresponding to the transition $2s2p^3\ ^3D_J^o \leftarrow 2s^22p^2\ ^3P_J$.[31,32,36] Because of self-absorption and self-reversal in the lamp and nonresonant emission from the (1,1) vibrational band of CO ($A^1\Pi \rightarrow X^1\Sigma^+$),[32] we had to perform calibration experiments to convert the measured absorbance into C-atom concentration. For this calibration, we carried out methane (99.995 %, Messer Griesheim) pyrolysis experiments at similar conditions as in the NCN experiments. The recorded absorbance-time profiles were compared to simulated C-atom concentration-time profiles obtained with a slightly changed version of the mechanism published by Dean and Hanson.[37] In this mechanism, we modified the rate coefficients of some of the reactions that affect the initial rising part of the C-atom profiles to better match the time of the measured and the simulated maximum of the C-atom concentration. Two new reactions were also added. The 36 reactions actually used and the

corresponding rate coefficients are listed in Table S3 of the Supporting Information along with the thermochemical data in Table S4.

At pressures of approximately 1 bar, the calibration experiments cover temperatures from 2630 up to 2970 K. Near 4 bar, we carried out calibration experiments at temperatures between 2760 and 3020 K. For the detailed reaction conditions see Tables S5 and S6 of the Supporting Information. The calibration curves are shown in Figures 1 and 2. As in earlier work,[38] the C-atom concentration-absorbance profiles for the higher pressures are steeper than those for the lower pressures. Since for a given pressure range (close to 1 bar and close to 4 bar, respectively) all the obtained calibration curves fell into a narrow range and did not show any discernible systematic temperature dependence (see Figures 1 and 2), we used averaged curves to calibrate the measured C-atom profiles in our NCN decomposition experiments.

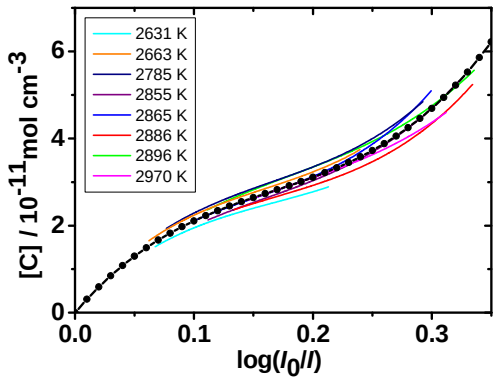

Figure 1. Calibration curves for different temperatures at pressures near 1 bar obtained with mixtures of 20 and 30.3 ppm CH_4 in Ar; (black dash-dotted line) averaged curve used in the NCN experiments.

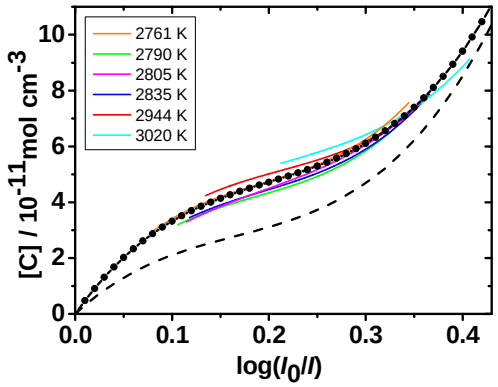

Figure 2. Calibration curves for different temperatures at pressures near 4 bar obtained with mixtures of 7.4 and 9.4 ppm CH_4 in Ar; (dash-dotted line) averaged curve used in the NCN experiments, (dashed line) averaged curve at 1 bar from Figure 1 for comparison.

We note in passing that we also tried to detect N atoms as a product of NCN decomposition.[23,24] We performed N-ARAS measurements (λ = 119.9 nm, lamp gas: 1% N_2 in He)[31,39] in the same temperature and pressure range as the C-ARAS measurements. However, calibration for these experiments at relatively low temperatures compared to other N-ARAS studies[31,39,40] turned out to be difficult. Using a calibration mixture of 200 to 300 ppm N_2O and 10% N_2 in Ar, we obtained calibration curves with a too large and strongly scattering temperature dependence that considerably differ from those of ref 39 and 40. Therefore, we refrained from inferring rate coefficients of the decomposition reaction NCN + M $\rightarrow$ N + CN + M, also because consecutive reactions producing N atoms cannot be ruled out. From the estimated, low N-atom yields, however, there is strong evidence that reaction R1 is indeed the by far dominating pathway of NCN decomposition. This was predicted in ref 18 and is also in line with the experimental results from ref 15 (see below).

2.3. Synthesis and Purity of Substances. Since NCN_3 is very explosive in solid and liquid form,[41] we adopted a synthesis described by Milligan et al.[42] that keeps NCN_3 in the gas phase (see also ref 14). This procedure is based on the reaction of NaN_3 (99%, Fluka) with BrCN (97%, Fluka) to produce NaBr and the desired NCN_3. The synthesis was carried out in an all-glass apparatus consisting of a 100 ml bulb equipped with a 25 cm long Vigreux column connected to a 2 l bulb. Before each synthesis, NaN_3 was finely powdered and immediately filled into the Vigreux column closed with glass wool. Then the entire apparatus was evacuated for several hours to remove air and volatile contaminants like water. It was then flushed with He, and some (less than 1 g) BrCN was put into the 100 ml glass bulb. After re-evacuation, BrCN was allowed to react under its own vapor pressure with NaN_3 for at least 15 hours. Gaseous NCN_3 was collected in the 2 L bulb and directly used to prepare the test mixture.

The obtained product was analyzed with IR spectroscopy and mass spectrometry. The spectra reveal a residual contamination with BrCN not exceeding 5%. Because variation of the initial concentrations in our shock tube experiments had no discernible influence on the rate coefficients of the NCN decomposition, we considered side reactions of BrCN as unimportant. Accordingly and in view of the problematic handling of NCN_3 in the condensed phase, we did not attempt further purification. We note, however, that the prepared mixtures of NCN_3 in Ar stored in stainless steel mixing vessels were not stable over a longer period. After a few days, we observed that the maxima of the C-atom concentration-time profiles in the shock-tube experiments decreased for identical initial reactant pressures. Conversely, the N atom concentrations increased. These effects are probably due to unwanted reactions of NCN_3 in the storage vessel. In mass-spectrometric analyses of the reactant mixtures (electron impact ionization, ionization energy: 45eV), we detected a signal at m/z 54 attributable to NCN_2 that

increased on a timescale of days. Furthermore, we found a small signal at *m*/*z* 80 which may be assigned to C_2N_4. Especially the latter signal seems to indicate the presence of association processes of NCN_3. Consequently, we used one mixture for at most three days. During this time, no systematic changes in the C-atom profiles were observed.

3. Computational Section

3.1. Quantum Chemical Calculations. The stationary points on the triplet potential energy surface of the CN_2 system proposed by Moskaleva and Lin[18] were re-optimized at several levels of theory including density functional theory[43] using the B3LYP combination of functionals,[44,45] in conjunction with the correlation-consistent triple-ζ basis set (cc-pVTZ) developed by Dunning *et al.*[46,47]. In addition, the geometries corresponding to each stationary point were optimized at the CCSD/cc-V*n*Z level of theory (with *n* = D,T).[47] At the geometries optimized at lower levels, CCSD(T)/cc-pVTZ and CCSD(T)/cc-pVQZ single-point energy calculations were performed, from which the complete basis set (CBS) limit was derived based on the extrapolation scheme proposed by Helgaker *et al.*[48]. For the extrapolation of the Hartree-Fock energies, we explicitly calculated them at all basis sets from cc-pVDZ to cc-pV6Z. In addition, potential energy surface scans were also performed at various levels of theory. All computations were performed with the GAUSSIAN03 suite of programs.[49]

3.2. Statistical Rate Theory Calculations. The rate coefficient of reaction R1 as a function of temperature and pressure was calculated as the lowest eigenvalue of the matrix **J** of an energy-resolved one-channel steady-state master equation:[29,30]

$$[\omega(\mathbf{I} - \mathbf{P}) + \mathbf{K}_1]\mathbf{N}^S \equiv \mathbf{J}\mathbf{N}^S = 0 \qquad (1)$$

Here, ω denotes the Lennard-Jones collision frequency, **I** is the unit matrix, **P** is the matrix of the collisional transition probabilities, $P(E, E')$, and $\mathbf{K}_1$ is a diagonal matrix of the specific rate coefficients, $k_1(E)$, with E being the internal energy of NCN counted from the rovibrational ground state. The vector $\mathbf{N}^S$ represents the steady-state population, $n^S(E;T,P)$, of NCN at a given temperature and pressure. The specific rate coefficients of reaction R1 were obtained from RRKM theory:[29,30]

$$k_1(E) = \frac{W_{\mathrm{TSB}}(E - E_0)}{h\rho_{\mathrm{NCN}}(E)} \qquad (2)$$

where h is Planck´s constant, $W_{\mathrm{TSB}}(E - E_0)$ is the sum of states of the transition state TSB of the rate-determining step (see below) with the corresponding threshold energy E_0, and $\rho_{\mathrm{NCN}}(E)$ denotes the density of states of NCN. All numbers and densities of states were determined by exact counting procedures[29,30,50,51] for a total angular momentum quantum number of J = 64, which is the thermally averaged J at a temperature of $T \sim 2400$ K corresponding to the middle of our experimental temperature range. We note that for the linear triatomic molecule NCN, also vibrational angular momentum coupling was accounted for.[52] The following harmonic wavenumbers (ω_i) and rotational constants (A, B) were used: NCN: ω_i = 1442, 1204, 459, 459 cm^{-1}, B = 0.397 cm^{-1} (linear molecule); TSB: ω_i = 1767, 700 cm^{-1}, A = 1.789 cm^{-1}, B = 0.748 cm^{-1} (approximated as prolate symmetric top). These data were obtained from our quantum chemical calculations at B3LYP/cc-pVTZ level of theory, where the wavenumbers were scaled by 0.9682.[53] A comparison with data from other authors and results from CCSD/VTZ calculations is made in Table S7 of the Supporting Information.

The collision frequency ω was calculated with the following parameters:[29,54] $\varepsilon(\mathrm{Ar})/k_B$ = 93.3 K, $\sigma(\mathrm{Ar})$ = 3.542 Å, $\varepsilon(\mathrm{NCN})/k_B \sim \varepsilon(\mathrm{CO_2})/k_B$ = 195.2 K, $\sigma(\mathrm{NCN}) \sim \sigma(\mathrm{CO_2})$ = 3.941 Å, where we

approximated the Lennard-Jones parameters of NCN by those of CO_2. For the transition probabilities in eq 1, a stepladder model obeying detailed balancing was used. The step size, ΔE_{SL}, was treated as a fitting parameter. The master equation was set up with a bin size of 10 cm^{-1}. The lowest eigenvalue was determined by standard routines for tridiagonal matrices.[55] More details and general aspects of our master equation code are given in refs 56 and 57.

4. Results and Discussions

4.1. Experiments. A typical C-atom concentration-time profile as obtained from our calibrated ARAS measurements is shown in Figure 3. The initial increase of the C-atom concentration is caused by reaction R1, and the rate coefficient k_1 was determined from a linear fit of a first-order rate law to the initial slope:

$$k_1 = \frac{1}{[\mathrm{NCN}]_0}\left(\frac{\mathrm{d}[\mathrm{C}]}{\mathrm{d}t}\right)_{t\to 0} \qquad (3)$$

We note that for longer reaction times, in the order of a few hundred microseconds depending on the initial concentration, the C-atom profiles started to decrease probably due to consecutive reactions. The initial slopes, however, were not influenced.

To check whether the rate coefficients k_1 are in the low-pressure limit, we calculated for each experimental point the bimolecular rate coefficient $k_1^{bim}(T,[\mathrm{Ar}]) = k_1(T,[\mathrm{Ar}])/[\mathrm{Ar}]$. The results are plotted in Figure 4. It is evident that the bimolecular rate coefficients are virtually independent of pressure, which indicates that the reaction is indeed at or very close to the low-pressure limit. The temperature dependence of k_1^{bim} can be expressed by the following Arrhenius equation:

$$k_1^{bim} = (4.2 \pm 2.1) \times 10^{14} \exp[-242.3\ \mathrm{kJ\ mol^{-1}}/(RT)]\ \mathrm{cm^3\ mol^{-1}\ s^{-1}} \qquad (4)$$

where the statistical error was estimated to be 50%. A systematic uncertainty may arise mainly from the calibration but is difficult to assess. In view of this combined uncertainty, we refrain

from giving a three-parameter Arrhenius-Kooij-type equation despite the slight curvature of the Arrhenius plot discernible in Figure 4.

Our experimentally determined rate coefficients agree very well with the results from Dammeier *et al.*[15]. The Arrhenius equation given in their work is also plotted in Figure 4. The rate coefficients virtually agree at the upper end of the temperature range near 3000 K and differ by about 40 % at the lower end near 1800 K. The temperature dependence found by Dammeier *et al.* (E_A = 260 kJ mol^{-1}) is a little bit stronger than that found in our experiments (E_A = 242.3 kJ mol^{-1}). These differences, however, are still within the combined uncertainty range of the experiments.

The very good agreement between the rate coefficients determined in this work with those from ref 15 can be seen as an indication that our calibration procedure is adequate. It provides also strong evidence for reaction R1 being indeed the dominant decomposition channel of NCN. Whereas in ref 15 the decay of NCN was monitored, in our experiments the production of C atoms was detected. If important parallel decomposition channels of NCN leading to products other than C existed, they would have led to differences in the rate coefficients determined with these two different methods. At least within the experimental uncertainties, such differences cannot be discerned.

In Figure 4, also the temperature dependence predicted by Moskaleva and Lin[18] is shown, and the agreement with the experimental results is good in particular at the higher temperatures.

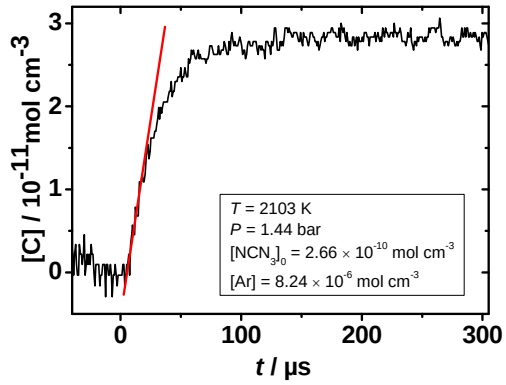

Figure 3. Experimental C-atom concentration-time profile (black line) and linear fit to the initial slope (red line).

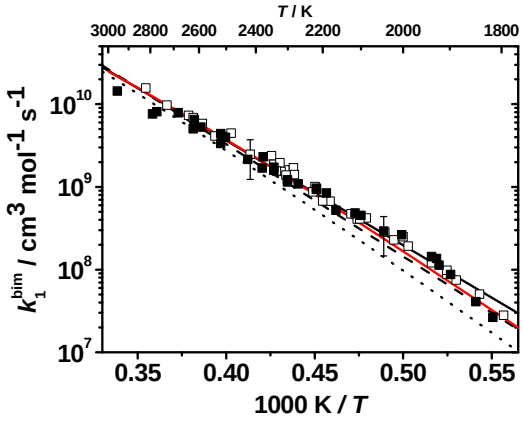

Figure 4. Temperature dependence of the second-order rate coefficient of reaction R1; (empty squares) experiments from this work at $P \sim 1$ bar; (solid squares) experiments from this work at $P \sim 4$ bar; (black solid line) fit to experimental data of this work, eq. 4; (black dashed line) fit to experimental data from ref 15; (black dotted line) prediction from ref 18; (red line) master equation simulation from this work (E_0 = 304.9 kJ mol^{-1}, ΔE_{SL} = 1500 cm^{-1}, see below).

In evaluating eq 3, the initial concentration of cyanonitrene, $[NCN]_0$, was assumed to be equal to the initial concentration of cyanogen azide, $[NCN_3]_0$. This assumption is warranted if NCN_3 decomposes comparatively fast and completely to NCN + N_2. In two recent investigations by

Friedrichs *et al.*,[25,26] it was conclusively shown that NCN_3 thermally dissociates to give ^{1}NCN + N_2 followed by collision-induced intersystem crossing (CIISC): $^1NCN + M \rightarrow {}^3NCN + M$. It turned out that at total argon densities of $(3–6) \times 10^{-6}$ mol cm^{-3}, which corresponds to pressures of e.g. 250–500 mbar at $T = 1000$ K, the collision-induced ISC becomes rate-determining for $T > 700$ K. Because the experimental data are limited to temperatures below 1250 K,[25,26] we estimated k_{CIISC} by extrapolating the Arrhenius expression given in ref 25 to the temperature range of our experiments. One obtains rate coefficients between $k_{CIISC} = 3.2 \times 10^{10}$ cm^3 mol^{-1} s^{-1} at $T = 1800$ K and 5.4×10^{10} cm^3 mol^{-1} s^{-1} at $T = 2900$ K, which is, except for the highest temperatures, well above the bimolecular rate coefficients of NCN decomposition, k_1^{bim} (cf. Figure 4), that is, the latter reaction is the rate-determining step.

At the initial stage of the NCN decomposition reaction, consecutive bimolecular reactions of the C atoms can be neglected due to the low initial NCN concentrations. We used mixtures with different initial NCN_3 concentrations (between 2 and 32.3 ppm, see Tables S1 and S2 of the Supporting Information) and did not find any systematic variation of the rate coefficients k_1 obtained.

4.2. Properties of the CN_2 Triplet Potential Energy Surface

The potential energies obtained at the CCSD(T)/CBS//CCSD/cc-pVTZ level of theory for the stationary points of the PES are shown in Figure 5, where TSC indicates the NN–C dissociation saddle point of Moskaleva and Lin.[18] Our calculations confirm that there is a well-defined saddle point in that part of the potential energy surface. However, a barrier of this height cannot be reconciled with the magnitude and pressure dependence of the experimental rate coefficients. To understand what is going on, the lowest triplet potential energy surface of the CN_2 system was

scanned as a function of the position of the C atom with respect to the center of mass of N_2 positioned in the origin of a Cartesian coordinate system, oriented along the *y* axis. The resulting plot calculated at the B3LYP/6-311G** level (used by Moskaleva and Lin to locate the decomposition saddle point)[18] is shown in Figure 6. The deep well of the PES corresponds to collinear CNN. One can see that there really is a saddle point at the geometry the earlier work reported.[18] In fact, not only one but two saddle points are located very close to each other. (This is specific to B3LYP. The PES obtained with the M06-2X functional, with CAS-SCF and with CCSD has only one saddle point in that region.) However, the high-energy decomposition saddle point is formed not because the weakening of the N–C bond is not compensated for by the strengthening of the N–N bond, as a qualitative picture could explain (see the principles of the bond energy-bond order method[58] and the conservation of bond order[59]). Instead, from the shape of the peak near the saddle point one can expect that the unusual feature of the PES is a reflection of a conical intersection. The upper cone has also been found by using time-dependent density functional theory (TD-DFT, B3LYP/6-311G**, at geometries far enough from the intersection where TD-DFT gave acceptable, converged results) and in full-valence CAS-SCF/cc-pVDZ calculations. The DFT potential energy surface correctly reflects the qualitative features of the PES in this region. Due to serious SCF convergence problems, only the calculations at the DFT level were productive enough to get large-density points in the extended range of Figures 6 and 7. However, calculations at other ab initio levels confined to the saddle-point region show that the shape of the PES is very similar to that in Figure 6. To get to this saddle point from the CNN potential well, the system needs a significant amount of energy. However, the plot also shows that the collinear departure of the carbon atom from the N_2 molecule needs much less energy, moreover, the energy remains below the level of the separated

fragments. Figure 7 shows the contour plot of the potential energy surface expanded to larger C–N_2 distances. A detailed scan of the collinear section of the PES performed at the CCSD(T)/aug-cc-pVQZ level indicates no barrier, except a submerged reef similar to earlier potential energy surfaces of O + O_2.[60] In Figure 7, a shallow "ditch" is visible, leading from the CNN well towards a T-shaped arrangement where the C atom is 3 Å from the center of mass of N_2. This is in fact a circular pathway around the N_2 molecule, corresponding to the identity reaction NNC to CNN, and is analogous to the roaming pathway of NCN isomerization to CNN reported by Harding *et al.*[22], where the N atom can roam around the CN radical. The relative energies of the potential energy surface agree within 4 kJ mol^{-1} with the MRCI data of Frankcombe *et al.*[20] except the cyclic isomer (which is 60 kJ mol^{-1} lower at our UCCSD(T) level) which does not play an important role in the mechanism. Based on these calculations, we can re-draw the potential energy profile of NCN decomposition in the CNN decomposition range; the result is shown in Figure 5. The rate-determining step is the isomerization of NCN via TSB to CNN and not the carbon loss from CNN via the bent transition state TSC. The carbon loss reaction along the asymptotic pathway will probably be very fast since the linear CNN is formed in the chemical activation ring-opening step with significant excess energy. Threshold energies for the rate-determining transition state TSB relative to NCN obtained with different quantum chemical methods are collected in Table 1.

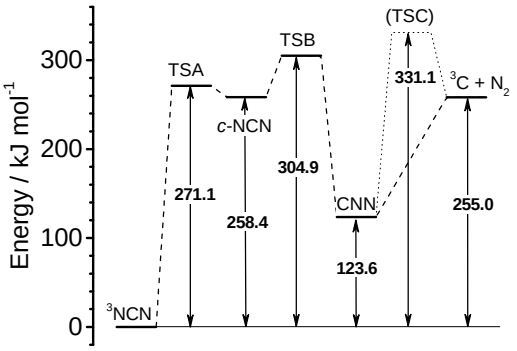

Figure 5. Potential energy diagram (zero-point corrected) calculated at the CCSD(T)/CBS//CCSD/cc-pVTZ level of theory.

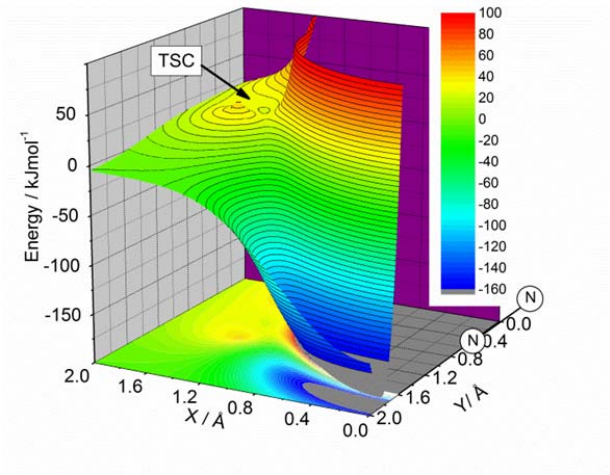

Figure 6. The potential energy surface of the lowest triplet state of CN_2 calculated as a function of the position of the carbon atom with respect to the center of mass of N_2 (marked by circles) oriented along the *y* axis at the B3LYP/6-311G** level of theory. The N–N distance is 1.144 Å corresponding to the saddle-point geometry. The collinear C–NN dissociation pathway proceeds along the *y* axis. The potential energy is measured from the level of the separated fragments.

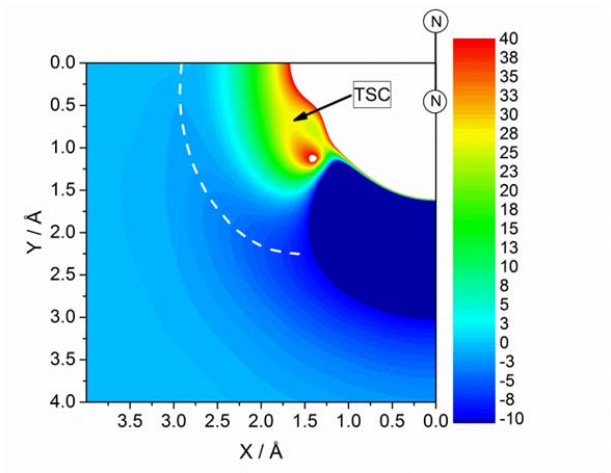

Figure 7. Same as Figure 6 spanning larger distances of the C atom from the center of mass of N_2. The collinear C–NN dissociation pathway proceeds along the *y* axis; the dashed white line indicates the roaming pathway.

Table 1. Threshold energy for TSB (see Figure 5) relative to NCN at 0 K.

E_0(TSB)/kJ mol^{-1}	method	reference
307.3	CCSD(T)/CBS//B3LYP/cc-pVTZ	this work
304.9	CCSD(T)/CBS//CCSD/cc-pVTZ	this work
301.2	(10E,9O)-CASPT2/cc-pVTZ	ref 22
307.8	RCCSD(T)/6-311G(d,p)//B3LYP/6-311G(d)	ref 18
320.5	B3LYP/6-311G(d,p)//B3LYP/6-311G(d)	ref 18
259.2	MP2/6-311G(d,p)//B3LYP/6-311G(d)	ref 18

253.9	MP2/6-311+G(3df,2p)//B3LYP/6-311G(d)	ref 18
309.2	PMP4/6-311G(d,p)//B3LYP/6-311G(d)	ref 18
305.3	G2M(RCC)	ref 18

4.3. Master Equation Modeling

A result of our master equation modeling is displayed in Figure 4. For this calculation, we used the threshold energy of E_0 = 304.9 kJ mol^{-1} obtained at CCSD(T)/CBS//CCSD/cc-pVTZ level of theory (*cf.* Table 1) and used ΔE_{SL} to fit the calculated rate coefficient to the measured points. We obtained the best fit with ΔE_{SL} = 1500 cm^{-1}. Fits of nearly identical quality were obtained with the following pairs of parameters: E_0 = 307.3 kJ mol^{-1} (CCSD(T)/CBS//B3LYP/cc-pVTZ) with ΔE_{SL} = 1670 cm^{-1} and E_0 = 301.2 kJ mol^{-1} ((10E,9O)-CASPT2/cc-pVTZ)[22] with ΔE_{SL} = 1400 cm^{-1}. The differences in the calculated rate coefficients for these three cases are well below 10%.

The master equation modeling confirms that the rate coefficient k_1 is very close to the low-pressure limit under our experimental conditions with deviations below −0.7% at pressures near 1 bar and below −2.2% near 4 bar. Extrapolations show that at a pressure of P = 10 bar, the deviation from the low-pressure limit is –7.4% at T = 1800 K, –3.1% at T = 2300 K, and –2.2% at T = 2900 K; the corresponding numbers at P = 50 bar are –19.6%, –12.9%, and –7.7%, respectively. As is obvious from Figure 4, the solution of the master equation also reproduces the slight negative curvature of the Arrhenius plot of the experimentally determined rate coefficients within their error margin. A parameterization of the results from our master equation calculations for selected pressures is given in Table S8 of the Supporting Information.

The fitted values for the parameter ΔE_{SL}, which represents the average energy transferred per down collision,[30] appear somewhat high for NCN-Ar collisions. However, this is a behavior often observed in thermally activated reactive systems where collisional energy transfer competes with unimolecular reaction steps.[30,61] Within the present work, we simply consider ΔE_{SL} as a parameter and do not attempt any quantitative interpretation. Otherwise, much more detailed models of collisional energy transfer, including an energy dependence of ΔE_{SL}, would have to be used. Such investigations are, however, beyond the scope of the present work and would require also a more detailed master equation that accounts for the multi-well character of the reaction system. Our experimental results may serve as a target to validate such models.

5. Summary and Conclusions

Shock-tube studies of the thermal decomposition of NCN have been performed with NCN_3 as a source of NCN and ARAS for monitoring concentration-time profiles of the ^3C atoms produced. The rate coefficients are in the range of 10^7–10^{10} cm^3 mol^{-1} s^{-1} at temperatures between 1800 and 2900 K. The rate coefficient and its temperature dependence were reproduced by master equation modeling with barrier heights and molecular data from quantum chemical calculations and an energy-transfer parameter as a fitting parameter. In agreement with the theoretical prediction of Moskaleva and Lin, the master equation modeling demonstrated that the reaction is in the low-pressure regime at 1 to 4 bar at temperatures above 2000 K and at 10 bar is still not far in the falloff region. The experimental data were not possible to fit with the entire mechanism of Moskaleva and Lin. Detailed studies of the potential energy surface showed that the key feature here is the barrier for carbon loss from the CNN intermediate. Instead of going via a relatively high-energy bent tight transition state, carbon loss can take place as a simple

bond fission reaction through a loose transition state along a collinear pathway. The potential energy surface also provides a roaming pathway for CNN to NNC isomerization. The calculations confirm that the overwhelming decomposition channel produces ^{3}C atoms.

The magnitude of the bimolecular decomposition rate coefficient is about four orders of magnitude lower than the rate coefficients measured for reactions of NCN with reactive species such as atomic oxygen in the high-temperature region. Considering that the concentration of stable molecules as nonreactive collision partners in flames is orders of magnitude larger than those of reactive species, the thermal decomposition of NCN as a NCN loss channel cannot be neglected.

Corresponding Author

*E-mail: matthias.olzmann@kit.edu.

Acknowledgments. Financial support by the Deutsche Forschungsgemeinschaft (SFB 606 "Non-Stationary Combustion: Transport Phenomena, Chemical Reactions, Technical Systems") is gratefully acknowledged. This work was supported in part by the Hungarian Scientific Research Fund (Grant No. K108966) and by the National Development Agency (Grant No. KTIA_AIK_12-1-2012-0014). The collaboration between the groups at KIT and the Hungarian Academy of Sciences was supported by the European Cooperation in Science and Technology (COST) within Action CM0901 "Detailed Chemical Kinetic Models for Cleaner Combustion". We also thank Prof. Gernot Friedrichs and his students for stimulating discussions.

Supporting Information. Experimental conditions and measured rate coefficients, calibration data, optimized geometries, calculated wavenumbers and rotational constants. This information is available free of charge via the Internet at http://pubs.acs.org.

References

(1) Moskaleva, L. V.; Lin, M. C. The Spin-Conserved Reaction CH + N_2 → H + NCN: A Major Pathway to Prompt NO Studied by Quantum/Statistical Theory Calculations and Kinetic Modeling of Rate Constant. *Proc. Combust. Inst.* **2000**, *28*, 2393−2401.

(2) Smith, G. P. Evidence of NCN as a Flame Intermediate for Prompt NO. *Chem. Phys. Lett.* **2003**, *367*, 541−548.

(3) El Bakali, A.; Pillier, L.; Desgroux, P.; Lefort, B.; Gasnot, L.; Pauwels, J. F.; da Costa, I. NO Prediction in Natural Gas Flames Using GDF-Kin®3.0 Mechanism NCN and HCN Contribution to Prompt-NO Formation. *Fuel* **2006**, *85*, 896−909.

(4) Sutton, J. A.; Williams, B. A.; Fleming, J. W. Laser-Induced Fluorescence Measurements of NCN in Low-Pressure $CH_4/O_2/N_2$ Flames and its Role in Prompt NO Formation. *Combust. Flame* **2008**, *153*, 465−478.

(5) Zsély, I. Gy.; Zádor, J.; Turányi, T. Uncertainty Analysis of NO Production During Methane Combustion. *Int. J. Chem. Kinet.* **2008**, *40*, 754−768.

(6) Konnov, A. A. Implementation of the NCN Pathway of Prompt-NO Formation in the Detailed Reaction Mechanism. *Combust. Flame* **2009**, *156*, 2093−2105.

(7) Lamoureux, N.; Desgroux, P.; El Bakali, A.; Pauwels, J. F. Experimental and Numerical Study of the Role of NCN in Prompt-NO Formation in Low-Pressure CH_4–O_2–N_2 and C_2H_2–O_2–N_2 Flames. *Combust. Flame* **2010**, *157*, 1929−1941 and (Corrigendum) **2013**, *160*, 745−746.

(8) Sutton, J. A.; Williams, B. A.; Fleming, J. W. Investigation of NCN and Prompt-NO Formation in Low-Pressure C1−C4 Alkane Flames. *Combust. Flame* **2012**, *159*, 562−576.

(9) Goos, E.; Sickfeld, C.; Mauß, F.; Seidel, L.; Ruscic, B.; Burcat, A.; Zeuch, T. Prompt NO Formation in Flames: The Influence of NCN Thermochemistry. *Proc. Combust. Inst.* **2013**, *34*, 657−666.

(10) Vasudevan, V.; Hanson, R. K.; Bowman, C. T.; Golden, D. M.; Davidson, D. F. Shock Tube Study of the Reaction of CH with N_2: Overall Rate and Branching Ratio. *J. Phys. Chem. A* **2007**, *111*, 11818−11830.

(11) Harding, L. B.; Klippenstein, S. J.; Miller, J. A. Kinetics of CH + N_2 Revisited with Multireference Methods. *J. Phys. Chem. A* **2008**, *112*, 522−532.

(12) Dagaut, P.; Glarborg, P.; Alzueta, M. U. The Oxidation of Hydrogen Cyanide and Related Chemistry. *Prog. Energy Combust. Sci.* **2008**, *34*, 1−46.

(13) Dammeier, J.; Friedrichs, G. Direct Measurements of the Rate Constants of the Reactions NCN + NO and NCN + NO_2 Behind Shock Waves. *J. Phys. Chem. A* **2011**, *115*, 14382−14390.

(14) Welz, O.; Olzmann, M. Kinetics of the NCN + NO Reaction over a Broad Temperature and Pressure Range. *J. Phys. Chem. A* **2012**, *116*, 7293−7301.

(15) Dammeier, J.; Faßheber, N.; Friedrichs, G. Direct Measurement of the High Temperature Rate Constant of the Reactions NCN + O, NCN + NCN, and NCN + M. *Phys. Chem. Chem. Phys.* **2012**, *14*, 1030−1037.

(16) Teng, W.-S.; Moskaleva, L. V.; Chen, H.-L.; Lin, M. C. Ab initio Chemical Kinetics for H + NCN Heat of Formation and Reaction Product Branching via Doublet and Quartet Surfaces. *J. Phys. Chem. A* **2013**, *117*, 5775−5784.

(17) Faßheber, N.; Dammeier, J.; Friedrichs, G. Direct Measurement of the Total Rate Constant of the Reaction NCN + H and Implications for the Product Branching Ratio and the Enthalpy of Formation of NCN. *Phys. Chem. Chem. Phys.* **2014**, *16*, 11647−11657.

(18) Moskaleva, L. V.; Lin, M. C. Computational Study on the Energetics of NCN Isomers and the Kinetics of the C + N_2 ⇔ N + CN Reaction. *J. Phys. Chem. A* **2001**, *105*, 4156−4163 (there are misprints in Table 7, the correct expression for the rate coefficient of the C + N_2 channel at 1 atm should read as: 3.26×10^{27} $(T/\mathrm{K})^{-4.76}$ $\exp(-41742\ \mathrm{K}/T)$ s^{-1}, for the NCN → CNN channel at 1 atm: 5.64×10^{28} $(T/\mathrm{K})^{-5.34}$ $\exp(-39464\ \mathrm{K}/T)$ s^{-1}, and at 133 mbar: 7.26×10^{27} $(T/\mathrm{K})^{-5.34}$ $\exp(-39457\ \mathrm{K}/T)$ s^{-1}, Moskaleva, L. V. private communication).

(19) Martin, J. M. L.; Taylor, P. R.; François, J. P.; Gijbels, R. Ab Initio Study of the Spectroscopy and Thermochemistry of the C_2N and CN_2 Molecules. *Chem. Phys. Lett.* **1994**, *226*, 475−483.

(20) Frankcombe, T. J.; McNeil, D. S.; Nyman, G. N + CN → C + N_2: A Global Potential Energy Surface, Entrance Channel Recrossing and the Applicability of Capture Theory. *Chem. Phys. Lett.* **2011**, *514*, 40−43.

(21) Ma, J.; Guo, H.; Dawes, R. Low Temperature Rate Constants for the N + CN → N_2 + C Reaction: Two-Dimensional Quantum Capture Calculations on an Accurate Potential Energy Suface. *Phys. Chem. Chem. Phys.* **2012**, *14*, 12090−12093.

(22) Harding, L. B.; Klippenstein, S. J.; Jasper, A. W. Separability of Tight and Roaming Pathways to Molecular Decomposition. *J. Phys. Chem. A* **2012**, *116*, 6967−6982.

(23) Busch, A.; Olzmann, M. Shock-Tube Study of the Thermal Decomposition of NCN. Proc. European Combust. Meeting 2009, Paper P810138.

(24) Busch, A. *Shock-Tube Studies on Decomposition Reactions of Nitrogen-Containing Compounds with Spectroscopic Methods*; PhD Thesis (in German), Karlsruher Institut für Technologie (KIT), KIT Scientific Publishing, 2010.

(25) Dammeier, J.; Friedrichs, G. Thermal Decomposition of NCN_3 as a High-Temperature NCN Radical Source: Singlet−Triplet Relaxation and Absorption Cross Section of NCN($^3\Sigma$). *J. Phys. Chem. A* **2010**, *114*, 12963−12971.

(26) Dammeier, J.; Oden, B.; Friedrichs, G. A Consistent Model for the Thermal Decomposition of NCN_3 and the Singlet−Triplet Relaxation of NCN. *Int. J. Chem. Kinet.* **2013**, *45*, 30−40.

(27) Just, Th. Atomic Resonance Absorption Spectrometry in Shock Tubes. In *Shock Waves in Chemistry*; Lifshitz, A., Ed.; Marcel Dekker: New York, 1981, p. 279−318.

(28) Michael, J. V.; Lifshitz, A. Atomic Resonance Absorption Spectroscopy with Flash or Laser Photolysis in Shock Wave Experiments. In: *Handbook of Shock Waves*; Ben-Dor, G.; Igra, O.; Elperin, T., Ed.; Vol. 3, Academic Press: San Diego, 2001, p. 77−105.

(29) Gilbert, R. G.; Smith, S. C. *Theory of Unimolecular and Recombination Reactions*; Blackwell: Oxford, 1990.

(30) Holbrook, K. A.; Pilling, M. J.; Robertson, S. H. *Unimolecular Reactions*, 2nd ed.; Wiley: Chichester, UK, 1996.

(31) Mozzhukhin, E.; Burmeister, M.; Roth, P. High Temperature Dissociation of CN. *Ber. Bunsen-Ges. Phys. Chem.* **1989**, *93*, 70−75.

(32) Dean, A. J.; Davidson, D. F.; Hanson, R. K. A Shock Tube Study of Reactions of C Atoms with H_2 and O_2 Using Excimer Photolysis of C_3O_2 and C Atom Atomic Resonance Absorption Spectroscopy. *J. Phys. Chem.* **1991**, *95*, 183−191.

(33) Bentz, T.; Giri, B. R.; Hippler, H.; Olzmann, M.; Striebel, F.; Szöri, M. Reaction of Hydrogen Atoms with Propyne at High Temperatures: An Experimental and Theoretical Study. *J. Phys. Chem. A* **2007**, *111*, 3812−3818.

(34) Gardiner, W. C., Jr.; Walker, B. F.; Wakefield, C. B. Mathematical Methods for Modeling Chemical Reactions in Shock Waves. In *Shock Waves in Chemistry*; Lifshitz, A., Ed.; Marcel Dekker: New York, 1981; p 319−374.

(35) Bak, B.; Bang, O.; Nicolaisen, F.; Rump, O. Assignment of Vibrational Frequencies in the Infrared and Raman Spectra of Cyanogen Azide. *Spectrochim. Acta A* **1971**, *27*, 1865−1871.

(36) Wiese, W. L.; Fuhr, J. R. Improved Critical Compilations of Selected Atomic Transition Probabilities for Neutral and Singly Ionized Carbon and Nitrogen. *J. Phys. Chem. Ref. Data* **2007**, *36*, 1287−1345.

(37) Dean, A. J.; Hanson, R. K. CH and C-Atom Time Histories in Dilute Hydrocarbon Pyrolysis: Measurements and Kinetics Calculations. *Int. J. Chem. Kinet.* **1992**, *24*, 517–532.

(38) Friedrichs, G.; Wagner, H. Gg. Investigation of the Thermal Decay of Carbon Suboxide. Z. Phys. Chem. **1998**, *203*, 1–14.

(39) Thielen, K.; Roth, P. Resonance Absorption Measurements of Nitrogen and Oxygen Atoms in High Temperature Nitric Oxide Dissociation and Formation Kinetics. *Proc. Combust. Inst.* **1984**, *20*, 685−693.

(40) Davidson, D. F.; Hanson, R. K. High Temperature Reaction Rate Coefficients Derived from N-Atom ARAS Measurements and Excimer Photolysis of NO. *Int. J. Chem. Kinet.* **1990**, *22*, 843–861.

(41) Marsh, F. D.; Hermes, M. E. Cyanogen Azide. *J. Am. Chem. Soc.* **1964**, *86*, 4506–4507.

(42) Milligan, D. E.; Jacox, M. E.; Bass, A. M. Matrix Isolation Study of the Photolysis of Cyanogen Azide. The Infrared and Ultraviolet Spectra of the Free Radical NCN. *J. Chem. Phys.* **1965**, *43*, 3149–3160.

(43) Parr, R. G.; Yang, W. *Density-functional Theory of Atoms and Molecules*; Oxford University Press: Oxford, 1989.

(44) Becke, A. D. Density-Functional Thermochemistry. III. The Role of Exact Exchange. *J. Chem. Phys.* **1993**, *98*, 5648–5652.

(45) Stephens, P. J.; Devlin, F. J.; Chabalowski, C. F.; Frisch, M. J. Ab Initio Calculation of Vibrational Absorption and Circular Dichroism Spectra Using Density Functional Force Fields. *J. Phys. Chem.* **1994**, 98, 11623−11627.

(46) Dunning, T. H., Jr. Gaussian Basis Sets for Use in Correlated Molecular Calculations. I. The Atoms Boron through Neon and Hydrogen. *J. Chem. Phys.* **1989**, *90*, 1007−1023.

(47) Kendall, R. A.; Dunning, T. H., Jr.; Harrison, R. J. Electron Affinities of the First-Row Atoms Revisited. Systematic Basis Sets and Wave Functions. *J. Chem. Phys.* **1992**, *96*, 6796−6806.

(48) Helgaker, T.; Klopper, W.; Koch, H.; Noga, J. Basis-Set Convergence of Correlated Calculations on Water. *J. Chem. Phys.* **1997**, *106*, 9639−9646.

(49) Frisch, M. J.; Trucks, G. W.; Schlegel, H. B.; Scuseria, G. E.; Robb, M. A.; Cheeseman, J. R.; Montgomery, Jr., J. A.; Vreven, T.; Kudin, K. N.; Burant, J. C. et al. *Gaussian 03*, revision C.02; Gaussian, Inc.: Wallingford, CT, 2004.

(50) Beyer, T.; Swinehart T. F. Algorithm 448: Number of Multiply-Restricted Partitions. *Comm. Assoc. Comput. Mach.* **1973**, *16*, 379−379.

(51) Troe, J. Specific Rate Constants k(E,J) for Unimolecular Bond Fission Reactions. *J. Chem. Phys.* **1983**, *79*, 6017−6029.

(52) Olzmann, M.; Troe, J. Approximate Determination of Rovibrational Densities of States $\rho(E,J)$ and Numbers of States $W(E,J)$. *Ber. Bunsen-Ges. Phys. Chem.* **1994**, *98*, 1563−1574.

(53) Merrick, J. P.; Moran, D.; Radom, L. An Evaluation of Harmonic Vibrational Frequency Scale Factors. *J. Phys. Chem. A* **2007**, *111*, 11683−11700.

(54) Reid, R. C.; Prausnitz, J. M.; Poling, B. E. *The Properties of Gases and Liquids*, 4th ed.; McGraw-Hill: Boston, U.S.A., 1987.

(55) Press, W. H.; Flannery, B. P.; Teukolski, S. A.; Vetterling, W. T. *Numerical Recipes in Fortran*, 2nd ed.; Cambridge University Press: Cambridge, UK, 1992.

(56) Olzmann, M. Statistical Rate Theory in Combustion: An Operational Approach. In: *Cleaner Combustion, Developing Detailed Chemical Kinetic Models*; Battin-Leclerc, F.; Simmie, J. N.; Blurock, E., Ed.; Springer: London, 2013, p. 549−576.

(57) Friedrichs, G.; Colberg, M.; Dammeier, J.; Bentz, T.; Olzmann, M. HCO Formation in the Thermal Unimolecular Decomposition of Glyoxal: Rotational and Weak Collision Effects. *Phys. Chem. Chem. Phys.* **2008**, *10*, 6520–6533.

(58) Johnston, H. S. *Gas Phase Reaction Rate Theory*, Ronald Press: New York, U.S.A., 1966.

(59) Lendvay, G. Bond Orders from Ab Initio Calculations and a Test of the Principle of Bond Order Conservation. *J. Phys. Chem.* **1989**, *93*, 4422–4429.

(60) Babikov, D.; Kendrick, B. K.; Walker, R. B.; Pack, R. T.; Fleurat-Lesard, P.; Schinke, R. Metastable States of Ozone Calculated on an Accurate Potential Energy Surface, *J. Chem. Phys.* **2003**, *118*, 6298−6308.

(61) Oref, I.; Tardy, D. C. Energy Transfer in Highly Excited Large Polyatomic Molecules. *Chem. Rev.* **1990**, *90*, 1407–1445.